Purification of 1.9-nm-diameter semiconducting single-wall carbon nanotubes using temperature-controlled gel-column chromatography and its application to thin-film transistor devices

Boanerges Thendie[1], Haruka Omachi[1], Jun Hirotani[2], Yutaka Ohno[2,3], Yasumitsu Miyata[4], and Hisanori Shinohara[1,5*]

[1]Department of Chemistry, Nagoya University, Nagoya 464-8602, Japan

[2]Department of Electrical Engineering and Computer Science, Nagoya University, Nagoya 464-8603, Japan

[3]Institute of Materials and Systems for Sustainability, Nagoya University, Nagoya 464-8603, Japan

[4]Department of Physics, Tokyo Metropolitan University, Hachioji, Tokyo 192-0397, Japan

[5]Institute of Advanced Research, Nagoya University, Nagoya 464-8602, Japan

[*]E-mail: noris@nagoya-u.jp

Large-diameter semiconductor single-wall carbon nanotubes (s-SWCNTs) have superior mobility and conductivity than those of small diameter s-SWCNTs. However, the purification of s-SWCNT with diameters larger than 1.6 nm by gel filtration has been difficult due to the low-selectivity of the conventional purification method in these large-diameter regions. We report a combination of temperature-controlled gel filtration and the gradient elution we developed to enrich high-purity s-SWCNT with a diameter as large as 1.9 nm. The thin-film transistor (TFT) device using the 1.9-nm-SWCNT shows an average channel mobility of 23.7 $cm^2V^{-1}s^{-1}$, which are much higher than those fabricated from the conventional SWCNT-TFTs with smaller diameters of 1.5 or 1.4 nm.

1. Introduction

Single-wall carbon nanotubes (SWCNTs) are superior semiconductor with high carrier mobility,[1-3] solution processability,[4-7] and excellent transparency and flexibility.[8-11] However, it is also known that the electronic properties of SWCNTs depend on their structure, which have broad varieties and are described basically by chirality, diameter, and length.[12, 13] Chirality of SWCNTs is defined by way of rolling a graphene sheet and determines their electronic type. One third of chirality distribution are metallic SWCNTs (m-SWCNTs) whereas other two third of the distribution are semiconducting SWCNTs (s-SWCNTs). The band gap of s-SWCNTs depends on the diameter with a decreasing tendency as the diameter increases.[14, 15] In addition, with increasing diameter, the carrier mobility and conductance of s-SWCNTs are expected to increase due to their decreasing band curvatures and increasing mean free path.[16, 17] The average length of SWCNT also plays an important role in film applications of SWCNTs such thin-film transistors (TFTs). In TFT, the length of SWCNT governs the number of inter-tube connects whose resistance are significantly higher than that of intra-tube resistance. As a result, this determines greatly the conductivity of TFT.[18-20] Furthermore, high-purity s-SWCNTs are also required for the electronic device fabrication. It is, therefore, highly desired to obtain large-diameter, long-length, and high-purity s-SWCNTs for semiconductor TFT device applications.[21-23]

Some sophisticated purification methods such as density gradient centrifugation[24], selective dispersion[25, 26], aqueous two phase extraction[27], and gel filtration[28-30] have been utilized to purify individual type of SWCNT. Among them, gel filtration is one of the most convenient methods for obtaining high-purity s-SWCNTs from its original mixture with m-SWCNTs. Aqueous dispersion of SWCNTs in a surfactant solution is

loaded onto gel column, which is then washed out by using surfactant solution. The SWCNTs are separated based on the difference of their elution speed[31] and preferential adsorption[32, 33] onto gel media. Purity over 99% of s-SWCNTs have been successfully obtained by this gel filtration method.[34, 35] Selectivity of s-SWCNTs purification has also been further improved by utilizing a series of multi-columns[36-38], allowing the enrichment of s-SWCNTs on single-chirality basis.

The use of gradual change of eluent composition to wash out s-SWCNTs (the so-called gradient elution) has also been reported to have a similar effect in increasing the selectivity for the purification based on diameter[39] as well as on chirality[40-42] of s-SWCNTs. In addition, due to the size exclusion effect of the gel column, the length-based purification of SWCNTs can be carried out as well, either as a separated[43, 44] or simultaneous process[45] with one on the basis of electronic-type. Most of reported successful purification of s-SWCNTs so far has been carried for small diameter SWCNTs with diameters less than 1.6 nm.[46] This is because of the fact that the conventional gel filtration has low selectivity in separating large-diameter s-SWCNTs.

Here, we report a successful purification of large-diameter s-SWCNTs by the gel filtration method utilizing a combination of temperature control and controlled low gradient elution (CLGE) technique we developed. Increasing temperature allows effective adsorption of large-diameter s-SWCNTs onto the gel column which are not achievable at room temperature, whereas the CLGE has been utilized to enhance electronic type and diameter based selectivity of the gel filtration. High-purity s-SWCNTs with an average diameter of as large as 1.9 nm have been successfully obtained using this combination method. The TFTs composed of this large-diameter s-SWCNT show improved carrier mobility and on-current density than those fabricated from sample with

smaller diameter of 1.5 and 1.4 nm.

2. Experimental methods

2.1. Sample preparation

Single-wall carbon nanotubes (SWCNTs) grown by direct injection pyrolytic synthesis (DIPS; Nikkiso Co., Ltd.) was used as the starting material[47]. A 1.0 mg/mL solution of the sample was then prepared by dispersing DIPS SWCNTs in aqueous solution of 1.0 wt% sodium cholate hydrate (SC 99%, Sigma-Aldrich) using bath sonicator (Nanoruptor NR-350, Cosmo Bio Co., Ltd.). Two dispersion conditions were utilized: a conventional dispersion which was carried out at a sonication power of 380 W for 10 h, and a weak dispersion which was carried out at a sonication power of 130 W for 1 h. The obtained solution was then centrifuged at 276,000 g for 1 h using a swing rotor (S52ST, Hitachi Koki) to remove undisperesed SWCNTs, and the upper 80% of the supernatant was collected as pristine SWCNTs (p-SWCNTs) sample.

2.2. Gel filtration

A small amount (1.0 mL) of pristine DIPS SWCNTs solution was mixed with same volume of 1.0 wt% sodium dodecyl sulfate (SDS 99%, Sigma-Aldrich) aqueous solution. The resulting solution was then loaded onto a jacketed column with inner-column diameter of 1 cm packed with 3 mL Allyl-dextran-based gel (Sephacryl S-100 HR, GE Healthcare) that had been saturated with an aqueous solution of 1.0 wt% SDS (cf. SI-1). Solution of SDS 1.0 wt% was then added to wash unadsorbed SWCNTs (mainly m-SWCNTs) out from the gel column. Subsequently, to collect SWCNTs adsorbed in the gel column (mainly s-SWCNTs), two different kinds of elution, a conventional way of

using fixed concentration of 1.0 wt% SC, and a CLGE system were utilized. The CLGE system setup, which was described in detail in the previous report,[48] utilizes V = 20 mL of 1.0 wt% SDS $[SDS]_0$ as the starting eluent and 1.0 wt% SC ($[SC]_0$) as modifier solution. The eluent was loaded into gel column at rate r of 1.1 mL/min. The SC concentration [*SC*] and the SDS concentration [*SDS*] in the eluent was described as function of elution time t expressed below:

$$[SC] = [SC]_0 \left[1 - \exp\left(-\frac{rt}{V}\right)\right] \quad (1)$$

$$[SDS] = [SDS]_0 \exp\left(-\frac{rt}{V}\right) \quad (2)$$

The sample was then collected as small fractions of ca. 0.6 mL each. During the whole gel filtration process, temperature-controlled water was flowed from a heated water bath in the outer-column to control the gel column temperature.

2.3. Fabrication of TFT

Fabrication of TFT has been done as described by Asada *et al.*[49] Silicon substrate with a 100 nm silicon oxide layer on the top side and a 10 nm titanium/100 nm gold layer on the back side was used as device substrate. Prior to SWCNT deposition, the substrate was treated by oxygen plasma and 3-aminopropyltriethoxysilane (APTES). Subsequently, 75 μL of the s-SWCNT solution was mixed with same volume of 1 wt% SC solution and then dropped onto the substrate. After the sample was left for overnight, the substrate was blow-dried by pressurized N_2 gas and washed by water overnight. The photolithography method was utilized to draw pattern on the substrate. Electrodes were fabricated by vapor deposition of 10 nm titanium followed by 100 nm gold in vacuum. Oxygen etching was then utilized to remove excess SWCNT film outside the device channel.

2.4. Characterization method

Each fraction of SWCNTs was spectroscopically characterized by measuring their optical absorption (JASCO V-570) and Raman spectra (Horiba Jobin Yvon HR-800). Diameter distribution was estimated from transmission electron microscopy (JEOL JEM-2100F) images of sample deposited on a copper grid, measured at 80 kV under vacuum (10^{-8} Torr). Film morphology and length of SWCNT were measured by atomic force microscopy (AFM; Veeco Nanoscope IV) in tapping mode. A semiconducting device analyzer (Agilen Technologies B1500A) was utilized to measure the electrical conductivity of sample at room temperature and open atmosphere condition.

3. Results and Discussion

As shown in Fig. 1, DIPS-SWCNT has a broad diameter distribution which ranges from 0.8 nm to 2.5 nm as measured from transmission electron microscopy (TEM). Because of this broad diameter distribution, the optical absorption peaks of m- and s-SWCNTs overlap each other and are difficult to identify, which results in an inability to quantitative assessment of s-SWCNTs purity on the basis of the optical absorption measurement.[50)]

3.1. Adsorption of large-diameter SWCNT

The effect of temperature on the adsorption of various diameter SWCNT onto the gel column has been investigated using conventionally dispersed p-SWCNTs at a power of 380 W for 10 h. The SWCNTs were adsorbed on the gel by 1 wt% SDS elution at various column temperature. During this SDS elution, s-SWCNTs are mainly adsorbed while the m-SWCNTs are mainly flowing-through the column. The adsorbed SWCNTs were then

collected by the conventional 1 wt% SC elution for their characterization. Figure 1 shows TEM images and the corresponding diameter distribution of the first SWCNT fraction from three different column temperatures of 16, 37, and 52 °C. These first fraction contains SWCNTs adsorbed weakly onto the gel column, which is a large-diameter portion within the SWCNT adsorbed (cf. SI-2).

The fractions of SWCNT eluted using conventional elution at a low column temperature of 16 °C contain only the smaller half of the p-SWCNT diameter distribution, indicating that large-diameter SWCNT has not been adsorbed by the gel column at this temperature. At 37 °C, similar fractions contain a large-diameter portion of the p-SWCNT. By increasing the column temperature up to 52°C, however, not only the largest diameter portion is adsorbed but a small diameter SWCNT ratio is also increased. We also found that the average diameter has not been changed much for the SWCNT fraction eluted at the temperatures higher than 37 °C. This temperature-dependent adsorption of SWCNT of the larger diameters than 1.6 nm is similar to a reported study by Liu *et al*[37] on the SWCNTs purification of the small diameters less than 1.0 μm.

The observed temperature-dependent adsorption of various diameter SWCNTs onto the gel column can be explained by using a thermodynamic approach as showed by Hirano *et al.*[51] The SWCNTs adsorption onto gel column is expressed by following reaction:

$$[\text{SWCNT} - \text{surfactant}]_{(aq)} + \text{gel} \rightleftharpoons n\ \text{surfactant}_{(aq)} + [\text{SWCNT} - \text{gel}]$$

The $[\text{SWCNT–surfactant}]_{(aq)}$ is the surfactant-stabilized SWCNT complex (solvated SWCNTs) in the solution (mobile phase) while [SWCNT–gel] is the SWCNT adsorbed on the gel (stationary phase). The equilibrium constant K of the reaction is defined from concentration of surfactant and [SWCNT–surfactant] as expressed by:

$$K = \frac{[\text{surfactant}_{(aq)}]^n}{[[\text{SWCNT}-\text{surfactant}]_{(aq)}]} \quad (3)$$

The thermodynamic of the process is therefore expressed by the Gibbs free energy ΔG equation derived from change of enthalpy ΔH and entropy ΔS:

$$\Delta G = \Delta H - T\Delta S = -RT \ln K \quad (4)$$

As also illustrated in Fig. 2, adsorption of an SWCNT onto gel dissociate SWCNT from the [SWCNT–surfactant] to form [SWCNT–gel]. The [SWCNT-gel] formation reduces the degree of freedom of SWCNT. However, the dissociation of [SWCNT–surfactant] (counted as a solvate) releases *n* surfactants per SWCNT, which increases the degree of freedom of surfactants. Due to their numbers, the increasing entropy of surfactants therefore exceeds the decreasing entropy of SWCNTs, increasing the overall entropy of the process ($\Delta S > 0$). In addition, the interaction between SWCNT and gel can be considered a hydrophobic one, which repels water molecules from the interfaces and contributes an increasing entropy in the adsorption process. Since the adsorption of SWCNT onto gel is entropy-driven, high-temperature therefore favor the process as it decreases the Gibbs free energy.

Interaction strength differences between SWCNT–surfactant and SWCNT–gel determine enthalpy change (ΔH) of the process. Strong dependences to the SWCNT diameter are expected for the SWCNT–surfactant interaction because diameter determines the SWCNT surface area and band gap. The latter determines SWCNT susceptibility to redox reaction and thus charge accumulation, which greatly affect Coulombic interaction of SWCNT–surfactant.[52-54)] Due to their large surface area and small band gap, large-diameter SWCNT are usually have stronger interaction with surfactant than small diameter one. Meanwhile, the SWCNT–gel interaction is assumed to have SWCNT-diameter dependency through surface area alone and lack Coulombic interaction due to the conventionally neutral gel matrix utilized. Thus, the ΔH is

dominated by SWCNT–surfactant interaction, and consequently the adsorption of large-diameter carbon nanotubes will have high ΔH compared to the adsorption of small-diameter ones. Consequently as demonstrated in this work, adsorption of the large-diameter SWCNTs requires high-temperature to compensate this high ΔH.

3.2. Selective desorption of s-SWCNT

The CLGE method we developed,[48] whose setup is illustrated in Fig. 3(b), is utilized to improve the purification of s-SWCNTs which schematic is shown in Fig. 3(a). As shown by the optical absorption spectra in Fig. 4(a), the SWCNT sample obtained by conventional SC elution at 37°C shows a strong optical absorption peak due to m-SWCNT around λ = 800 nm. By utilizing the CLGE method, the m-SWCNT peak was significantly reduced, indicating an increased purity of s-SWCNTs due to the low gradient change of surfactant composition in eluent as shown in Fig. 3(b). Raman spectra at an excitation wavelength λ_{ex} = 633 nm of the sample eluted by SC elution and the CLGE method are shown in Fig. 4(b). The SWCNT eluted by the CLGE exhibits a strong s-SWCNT peak with almost complete absence of the m-SWCNT peak, which can be contrasted with the SC elution counterpart where s- and m-SWCNT peaks have similarly been observed (cf. SI-3).

Figure 4(c) shows a TEM image and diameter distribution of the sample eluted by the CLGE method at 37°C. Compared to the SC elution case shown in Fig. 1, the SWCNT has a similar average diameter, but a much narrower distribution, indicating an improved diameter-sorting selectivity. As reported previously, CLGE increases separation selectivity not only on the basis of electronic-type, but also on the basis of SWCNTs diameter.[48] In the present work which utilizes wide distribution of SWCNTs diameter,

this improved selectivity of diameter sorting may have important role in the purity improvement of DIPS s-SWCNT eluted by CLGE. Raman spectra at λ_{ex} = 633 nm conventionally eluted fractions confirms the coexistence of m-SWCNTs with diameter of 1.2 nm and s-SWCNTs with diameter of 1.7 nm. In fractions collected by CLGE, the 1.2-nm-diameter m-SWCNTs are collected at much later fractions than the 1.7-nm-diameter s-SWCNTs, improving the s-SWCNTs purity. However, m-SWCNTs with diameter of 1.6 nm are confirmed still coexisting with the 1.7-nm-diameter s-SWCNTs i.e., in the first fraction obtained by CLGE, indicating diameter-sorting role in the improved s-SWCNTs enrichment (cf. SI-3).

3.3. Purification of weakly dispersed sample

Although long s-SWCNTs have been highly required for their TFT device application, the conventional dispersion method normally utilizes strong sonication that fractures, shortens and even damages SWCNTs[55]. To prevent these, a weak dispersion is incorporated by using a low sonication power of 130 W with a short dispersion time of 1 h. Figure 5 presents the AFM images p-SWCNTs prepared by conventional and the weak dispersion condition prior to any purification. The average length of the weakly dispersed p-SWCNT is 0.78 μm, which is almost double the value of the conventionally dispersed p-SWCNT. The ratio of micrometer-long SWCNT (SWCNT length > 1 μm) contents also seven times higher in the weakly dispersed p-SWCNTs (ca. 29%) than the conventional dispersed p-SWCNTs (ca. 4%). On the other hand, the concentration of SWCNTs in the weakly dispersed p-SWCNT are lower than the conventional one (cf. SI-4).

Purification of s-SWCNT from a weakly dispersed p-SWCNT shows intriguing results. Figure 6(a) shows the schematic of s-SWCNTs purification from weakly dispersed

sample using CLGE at 37°C. Optical absorption spectra of the first s-SWCNT fraction obtained by the method is shown in Fig. 6(b), in comparison with the conventional one. The peaks due to s-SWCNT in the first fraction obtained from the weakly dispersed p-SWCNTs are appeared at longer wavelengths than those obtained from the conventional one, indicating contents of larger-diameter s-SWCNTs. The m-SWCNT peak is not clearly visible in the fraction obtained from the weakly dispersed sample, showing a much increased purity of s-SWCNT, which is also confirmed by Raman spectra (cf. SI-5).

Figure 7 shows a typical TEM image of the first s-SWCNTs fraction obtained by CLGE at 37°C from the weakly dispersed p-SWCNTs. The s-SWCNTs obtained from this weakly dispersed sample have average diameter of 1.9 nm, which is larger than those obtained from the conventionally dispersed p-SWCNTs. The low SWCNT concentration in weakly dispersed p-SWCNTs is expected to have an important role in this adsorption of large-diameter s-SWCNT, where at low concentration SWCNTs were less competing with each other to be adsorbed on the gel surface.

3.4. Thin-film transistor applications

TFTs have been fabricated from s-SWCNTs, which are obtained by CLGE method from weakly dispersed p-SWCNTs, to evaluate the present purification of s-SWCNTs. Figure 8(a) shows transfer characteristic of TFTs with a channel length and a channel width of 100 μm and 100 μm, respectively. The TFTs are fabricated from the s-SWCNT with a diameter of 1.9 nm which is obtained from purification at 37°C. The devices exhibit an on/off ratio of 5 x 10^4 with an average channel mobility of 3.6 and 11.0 $cm^2V^{-1}s^{-1}$ as calculated by the so-called parallel plate and rigorous[56] model, respectively. The rigorous model takes the SWCNT film density into account when calculating the channel mobility.

The large difference between mobilities of the two models is due to a low density of SWCNT as indicated by the AFM image shown in Fig. 8(b).

Figure 9 and table I summarize the transfer properties of TFTs fabricated from three different diameter s-SWCNTs of 1.4, 1.5, and 1.9 nm as confirmed by their TEM images (cf. SI-6). These s-SWCNTs are obtained as first fraction of CLGE at 24, 30, and 37°C from the weakly dispersed p-SWCNTs, respectively. It should be noted that the 1.9 nm SWCNT is the same as that previously discussed but its film density is increased about three times than those shown in Fig. 8. All of the TFTs measurements are carried out at a channel length of 100 μm and a channel width of 100 μm with a drain-source voltage V_{DS} = 0.5 V (cf. SI-7). TFTs fabricated from the s-SWCNT with a diameter of 1.9 nm exhibit the channel mobility of 15.4 and 23.7 $cm^2V^{-1}s^{-1}$ as calculated by parallel plate and rigorous model, respectively. This channel mobility is much higher than those fabricated from smaller diameter s-SWCNT sample. Among the TFTs measured, those fabricated from 1.9-nm-diameter s-SWCNT also exhibit the highest channel on-current density of 27 μAmm^{-1} at a gate voltage of -10 V. On the other hand, the on/off ratio of 1.9-nm-diameter s-SWCNT devices is an order of magnitude smaller than those fabricated from smaller diameter sample. This low on/off ratio is due to the increased off-current of large-diameter SWCNT TFTs of the order of 10^{-9} A. As discussed previously, the 1.9-nm s-SWCNTs TFTs with a low-density film has a low off-current of the order of 10^{-11} A and the on/off ratio of an order of magnitude higher than the high-density TFT. The increased off-current in the high-density film of 1.9 nm s-SWCNTs is, therefore, due to increasing SWCNTs bundles, which substantially reduces electrical field effects[57]. This bundle screening combined with their proneness to unintentional electrical doping from its environment (i.e., oxygen in air[58] and remaining surfactant[59]) increases the off-current

of large-diameter SWCNTs TFTs.

The observed superior carrier mobility and on-current density can ensure that large-diameter s-SWCNTs are worthwhile to be utilized in TFT applications as predicted by theoretical calculation.[16] Also, as demonstrated by Asada *et al.*[60], the TFTs from unpurified samples show opposite results where large-diameter SWCNT shows smallest mobility. The present results show that purification processes are essential to realize high-performance applications of large-diameter s-SWCNTs.

4. Conclusions

Purification of large-diameter s-SWCNTs by gel-filtration requires high-temperature and selective elution, i.e. CLGE method. The high-temperature is essential to adsorb large-diameter s-SWCNTs on the gel column for their purification. The CLGE method has been utilized to improve the typically low selectivity elution of large-diameter s-SWCNT in the basis of diameter and electronic type. High-purity s-SWCNT with an average diameter of 1.9 nm has been obtained from a weakly dispersed p-SWCNTs by CLGE at 37°C. Transfer properties of TFTs fabricated from the 1.9 nm s-SWCNT exhibit much better device properties over those fabricated from smaller diameter SWCNTs, showing a carrier mobility of 23.7 $cm^2V^{-1}s^{-1}$.

Acknowledgments

The present study has been supported by “Indium-replacement by single-wall carbon nanotubes” (IRENA) of Europa Union and JST Japan and by MEXT/JSPS KAKENHI Grant Number JP16H06350. B.T. acknowledges support from Grant-in-Aid for JSPS Fellows Grant Number JP26011197.

References

1) T. Dürkop, S. A. Getty, E. Cobas, and M. S. Fuhrer, Nano Lett. **4**, 35 (2004).

2) S. J. Kang, C. Kocabas, T. Ozel, M. Shim, N. Pimparkar, M. A. Alam, S. V. Rotkin, and J. A. Rogers, Nat Nano **2**, 230 (2007).

3) X. Duan, C. Niu, V. Sahi, J. Chen, J. W. Parce, S. Empedocles, and J. L. Goldman, Nature **425**, 274 (2003).

4) M. F. Islam, E. Rojas, D. M. Bergey, A. T. Johnson, and A. G. Yodh, Nano Lett. **3**, 269 (2003).

5) M. A. Meitl, Y. Zhou, A. Gaur, S. Jeon, M. L. Usrey, M. S. Strano, and J. A. Rogers, Nano Lett. **4**, 1643 (2004).

6) H. Okimoto, T. Takenobu, K. Yanagi, Y. Miyata, H. Shimotani, H. Kataura, and Y. Iwasa, Adv. Mater. **22**, 3981 (2010).

7) Y. Nobusa, Y. Yomogida, S. Matsuzaki, K. Yanagi, H. Kataura, and T. Takenobu, Appl. Phys. Lett. **99**, 183106 (2011).

8) P. H. Lau, K. Takei, C. Wang, Y. Ju, J. Kim, Z. Yu, T. Takahashi, G. Cho, and A. Javey, Nano Lett. **13**, 3864 (2013).

9) Q. Cao, H.-s. Kim, N. Pimparkar, J. P. Kulkarni, C. Wang, M. Shim, K. Roy, M. A. Alam, and J. A. Rogers, Nature **454**, 495 (2008).

10) Q. Cao, S. H. Hur, Z. T. Zhu, Y. G. Sun, C. J. Wang, M. A. Meitl, M. Shim, and J. A. Rogers, Adv. Mater. **18**, 304 (2006).

11) E. Artukovic, M. Kaempgen, D. S. Hecht, S. Roth, and G. Grüner, Nano Lett. **5**, 757 (2005).

12) R. Saito, M. Fujita, G. Dresselhaus, and M. S. Dresselhaus, Appl. Phys. Lett. **60**, 2204 (1992).

13) J. W. Mintmire and C. T. White, Phys. Rev. Lett. **81**, 2506 (1998).

14) J. W. Ding, X. H. Yan, and J. X. Cao, Physical Review B **66**, 073401 (2002).

15) J. W. Mintmire and C. T. White, Carbon **33**, 893 (1995).

16) Y. Zhao, A. Liao, and E. Pop, IEEE Electron Device Letters **30**, 1078 (2009).

17) X. Zhou, J.-Y. Park, S. Huang, J. Liu, and P. L. McEuen, Phys. Rev. Lett. **95**, 146805 (2005).

18) C. Li, E. T. Thostenson, and T.-W. Chou, Appl. Phys. Lett. **91**, 223114 (2007).

19) P. N. Nirmalraj, P. E. Lyons, S. De, J. N. Coleman, and J. J. Boland, Nano Lett. **9**, 3890 (2009).

20) D. Simien, J. A. Fagan, W. Luo, J. F. Douglas, K. Migler, and J. Obrzut, ACS Nano **2**, 1879 (2008).

21) S. Fujii, T. Tanaka, Y. Miyata, H. Suga, Y. Naitoh, T. Minari, T. Miyadera, K. Tsukagoshi, and H. Kataura, Applied Physics Express **2**, 071601 (2009).

22) J. Wu, L. Xie, G. Hong, H. E. Lim, B. Thendie, Y. Miyata, H. Shinohara, and H. Dai, Nano Research **5**, 388 (2012).

23) Y. Kuwahara, F. Nihey, S. Ohmori, and T. Saito, Carbon **91**, 370 (2015).

24) M. S. Arnold, A. A. Green, J. F. Hulvat, S. I. Stupp, and M. C. Hersam, Nat Nano **1**, 60 (2006).

25) F. Toshimitsu and N. Nakashima, Nature Communications **5**, 5041 (2014).

26) T. Fukumaru, F. Toshimitsu, T. Fujigaya, and N. Nakashima, Nanoscale **6**, 5879 (2014).

27) C. Y. Khripin, J. A. Fagan, and M. Zheng, J. Am. Chem. Soc. **135**, 6822 (2013).

28) K. Moshammer, F. Hennrich, and M. M. Kappes, Nano Research **2**, 599 (2009).

29) M. Zheng, A. Jagota, M. S. Strano, A. P. Santos, P. Barone, S. G. Chou, B. A. Diner,

M. S. Dresselhaus, R. S. McLean, G. B. Onoa, G. G. Samsonidze, E. D. Semke, M. Usrey, and D. J. Walls, Science **302**, 1545 (2003).

30) T. Tanaka, Y. Urabe, D. Nishide, and H. Kataura, Applied Physics Express **2**, 125002 (2009).

31) D. A. Heller, R. M. Mayrhofer, S. Baik, Y. V. Grinkova, M. L. Usrey, and M. S. Strano, J. Am. Chem. Soc. **126**, 14567 (2004).

32) A. Hirano, T. Tanaka, and H. Kataura, The Journal of Physical Chemistry C **115**, 21723 (2011).

33) A. Hirano, T. Tanaka, Y. Urabe, and H. Kataura, ACS Nano **7**, 10285 (2013).

34) Y. Miyata, K. Shiozawa, Y. Asada, Y. Ohno, R. Kitaura, T. Mizutani, and H. Shinohara, Nano Research **4**, 963 (2011).

35) G. S. Tulevski, A. D. Franklin, and A. Afzali, ACS Nano **7**, 2971 (2013).

36) H. Liu, T. Tanaka, and H. Kataura, physica status solidi (b) **248**, 2524 (2011).

37) H. Liu, T. Tanaka, Y. Urabe, and H. Kataura, Nano Lett. **13**, 1996 (2013).

38) K. Tvrdy, R. M. Jain, R. Han, A. J. Hilmer, T. P. McNicholas, and M. S. Strano, ACS Nano **7**, 1779 (2013).

39) H. Liu, Y. Feng, T. Tanaka, Y. Urabe, and H. Kataura, The Journal of Physical Chemistry C **114**, 9270 (2010).

40) H. Gui, H. Li, F. Tan, H. Jin, J. Zhang, and Q. Li, Carbon **50**, 332 (2012).

41) B. S. Flavel, K. E. Moore, M. Pfohl, M. M. Kappes, and F. Hennrich, ACS Nano **8**, 1817 (2014).

42) Y. Yomogida, T. Tanaka, M. Zhang, M. Yudasaka, X. Wei, and H. Kataura, Nature Communications **7**, 12056 (2016).

43) D. Chattopadhyay, S. Lastella, S. Kim, and F. Papadimitrakopoulos, J. Am. Chem.

Soc. **124**, 728 (2002).

44) X. Huang, R. S. McLean, and M. Zheng, Anal. Chem. **77**, 6225 (2005).

45) B. Thendie, Y. Miyata, R. Kitaura, Y. Miyauchi, K. Matsuda, and H. Shinohara, Applied Physics Express **6**, 065101 (2013).

46) F. Hennrich, W. Li, R. Fischer, S. Lebedkin, R. Krupke, and M. M. Kappes, ACS Nano **10**, 1888 (2016).

47) H. Ago, S. Ohshima, K. Uchida, and M. Yumura, The Journal of Physical Chemistry B **105**, 10453 (2001).

48) T. Boanerges, O. Haruka, M. Yasumitsu, and S. Hisanori, Jpn. J. Appl. Phys. **56**, 015101 (2017).

49) Y. Asada, Y. Miyata, Y. Ohno, R. Kitaura, T. Sugai, T. Mizutani, and H. Shinohara, Adv. Mater. **22**, 2698 (2010).

50) Y. Miyata, K. Yanagi, Y. Maniwa, and H. Kataura, The Journal of Physical Chemistry C **112**, 13187 (2008).

51) A. Hirano, T. Tanaka, and H. Kataura, ACS Nano **6**, 10195 (2012).

52) A. Hirano, T. Kameda, Y. Yomogida, M. Wada, T. Tanaka, and H. Kataura, ChemNanoMat **2**, 911 (2016).

53) J. G. Duque, C. G. Densmore, and S. K. Doorn, J. Am. Chem. Soc. **132**, 16165 (2010).

54) H. Gui, J. K. Streit, J. A. Fagan, A. R. Hight Walker, C. Zhou, and M. Zheng, Nano Lett. **15**, 1642 (2015).

55) H. Shirae, D. Y. Kim, K. Hasegawa, T. Takenobu, Y. Ohno, and S. Noda, Carbon **91**, 20 (2015).

56) Q. Cao, M. Xia, C. Kocabas, M. Shim, J. A. Rogers, and S. V. Rotkin, Appl. Phys.

Lett. **90**, 023516 (2007).

57) L. Nilsson, O. Groening, C. Emmenegger, O. Kuettel, E. Schaller, L. Schlapbach, H. Kind, J.-M. Bonard, and K. Kern, Appl. Phys. Lett. **76**, 2071 (2000).

58) P. G. Collins, K. Bradley, M. Ishigami, and A. Zettl, Science **287**, 1801 (2000).

59) L. Hong, F. Toshimitsu, Y. Niidome, and N. Nakashima, Journal of Materials Chemistry C **2**, 5223 (2014).

60) Y. Asada, F. Nihey, S. Ohmori, H. Shinohara, and T. Saito, Adv. Mater. **23**, 4631 (2011).

Figure captions

Fig. 1. (Color online) (a) Typical TEM images and (b) the correspondent diameter distribution histograms of pristine DIPS SWCNT (p-SWCNT) and first fraction of s-SWCNT eluted conventionally from column temperature of 16°C, 37°C, and 52°C. The scale bars in TEM images are 5 nm and the average diameter (d_t) of SWCNTs are shown in each histogram.

Fig. 2. (Color online) Illustration of adsorption process of an SWCNT onto a gel bead where surfactants are relieved from the SWCNT surface, increasing entropy ($\Delta S>0$) of the system. The enthalpy (H) of the process changes as the SWCNT changes its interaction from with surfactants to with gel.

Fig. 3. (Color online) (a) Schematic of s-SWCNTs enrichment from the conventionally dispersed p-SWCNTs using CLGE at 37°C. (b) Illustration of the CLGE setup and (c) a plot of SC concentration in CLGE vs. elution time obtained from experimental data (red circle) and theoretical calculation (black line). The timing of s-SWCNT collection is also indicated (red shade area).

Fig. 4. (Color online) (a) Optical absorption and (b) Raman spectra showing differences in purity of the first s-SWCNT fraction obtained by conventional SC elution (red line) and CLGE (blue line) at 37°C. The spectrum of p-SWCNT is also shown as reference (black line). (c) TEM image and diameter distribution of first s-SWCNT fraction eluted by CLGE. The Gaussian fitting of the SWCNT diameter distribution obtained by

conventional elution (orange-shaded color) and CLGE (blue-shaded color) is also shown. The scale bar of the TEM image is 5 nm.

Fig. 5. (Color online) Atomic force microscopy (AFM) images of p-SWCNTs dispersed by (a) conventional at 380 W for 10 h, and (b) weak sonication at 130 W for 1 h prior to any purification. The length distributions of each p-SWCNT samples are shown below their respective AFM images. The average length (l_t) is also shown in each histogram and the scale bars are 2 μm.

Fig. 6. (Color online) (a) Schematic of large-diameter s-SWCNTs enrichment from the weakly dispersed p-SWCNTs using CLGE at 37°C. (b) As-measured optical absorption spectrum of first s-SWCNTs fraction obtained by the method (green). A spectrum of s-SWCNTs obtained with similar method (CLGE, 37°C) from conventionally dispersed sample (blue) is also shown as reference.

Fig. 7. (Color online) (a) TEM image and diameter distribution of the first s-SWCNTs fraction obtained from the method shown in Fig. 5, diameter of which are 1.9 nm in average. The scale bar is 5 nm.

Fig. 8. (Color online) (a) Transfer characteristic of thin film transistor (TFT) devices fabricated from s-SWCNTs with large-diameter of 1.9 nm, measured at drain voltage V_{DS} = 0.5 V. (b) AFM image and the corresponding height profile, with scale bar of 2 μm.

Fig. 9. (Color online) Summary plot of high density TFTs fabricated from s-SWCNTs

with various diameter of 1.4 (triangle), 1.5 (circle), and 1.9 nm (square). The *x* axis is on/off ratio while *y* axis is (c) channel mobility and (d) on-current density. The channel mobility shown was calculated using rigorous model.

Table I Characteristics of TFTs fabricated from three s-SWCNTs sample obtained by CLGE at different column temperatures.

Purification temperature / °C	24	30	37
Average tube diameter / nm	1.4 ± 0.3	1.5 ± 0.2	1.9 ± 0.2
On/off ratio	$2 \pm 1 \times 10^4$	$4 \pm 3 \times 10^4$	$4 \pm 1 \times 10^3$
On-current density / $\mu A mm^{-1}$	13 ± 2	18 ± 2	27 ± 2
Carrier mobility / $cm^2V^{-1}s^{-1}$ (parallel plate model)	8.2 ± 1.1	10.1 ± 0.7	15.4 ± 1.4
Carrier mobility / $cm^2V^{-1}s^{-1}$ (rigorous model)	13.7 ± 1.4	14.4 ± 1.0	23.7 ± 1.4

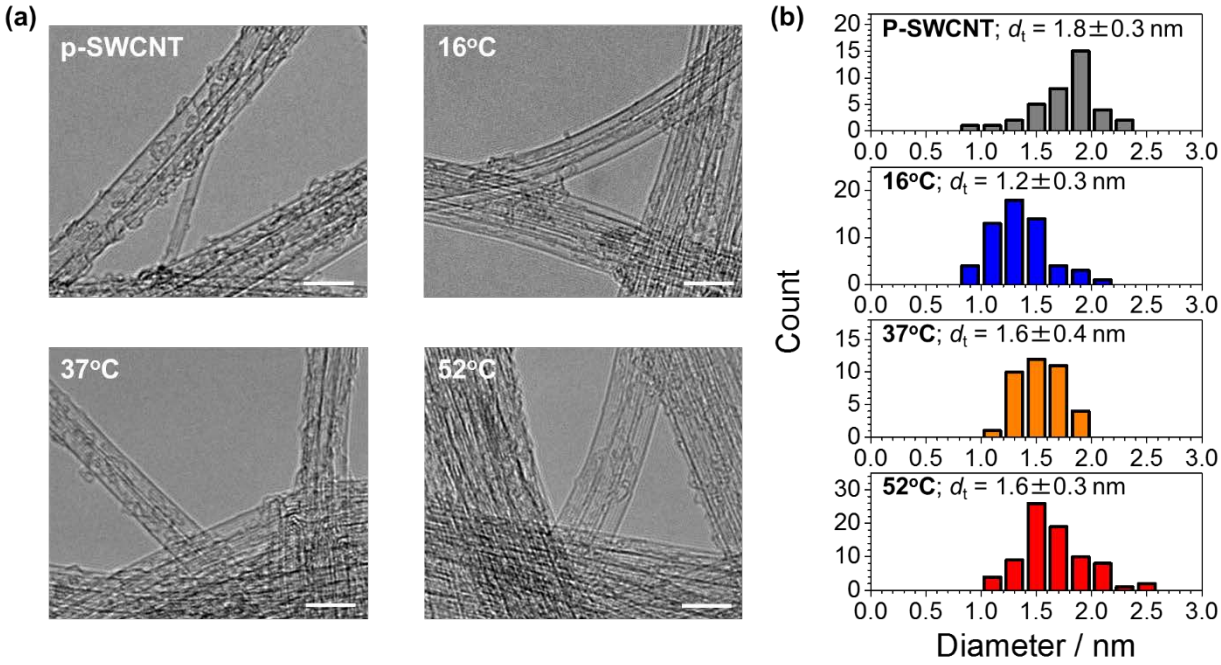
(a)
p-SWCNT
16°C
37°C
52°C
(b)
P-SWCNT; d_t = 1.8±0.3 nm
16°C; d_t = 1.2±0.3 nm
37°C; d_t = 1.6±0.4 nm
52°C; d_t = 1.6±0.3 nm
Count
Diameter / nm

Fig. 1.

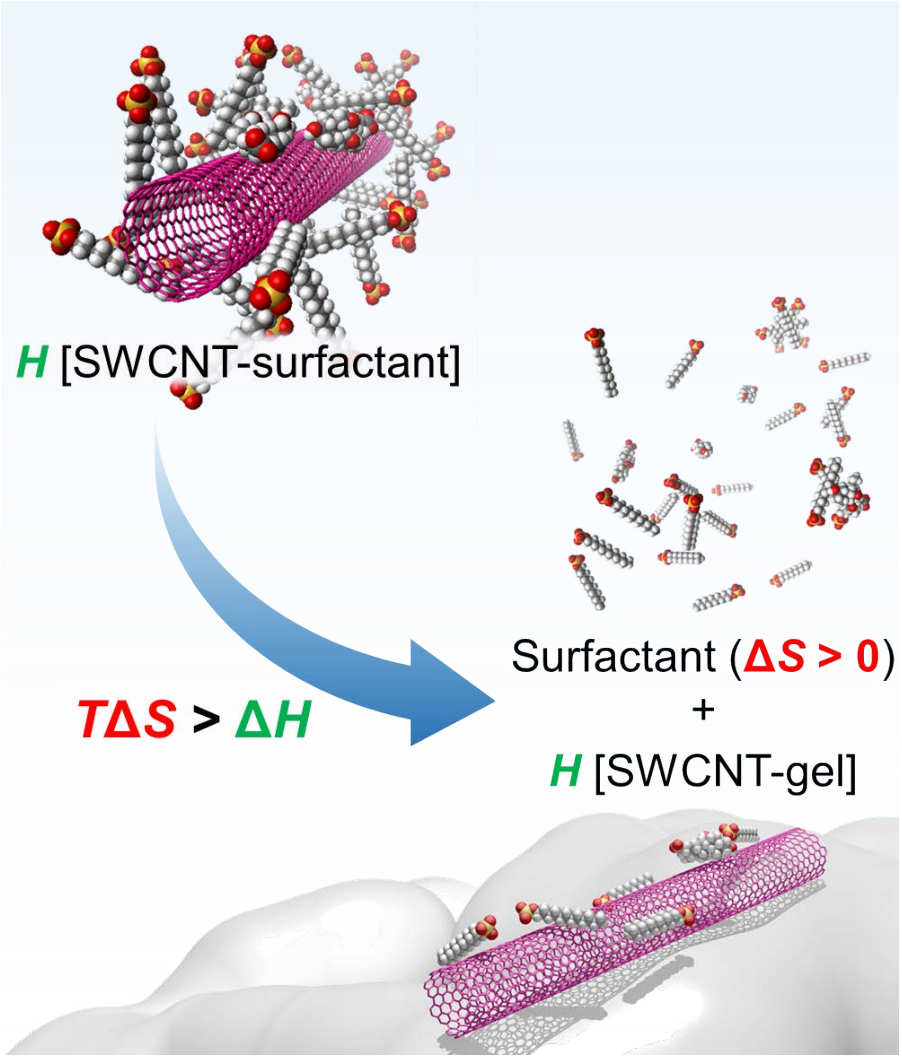

Fig. 2.

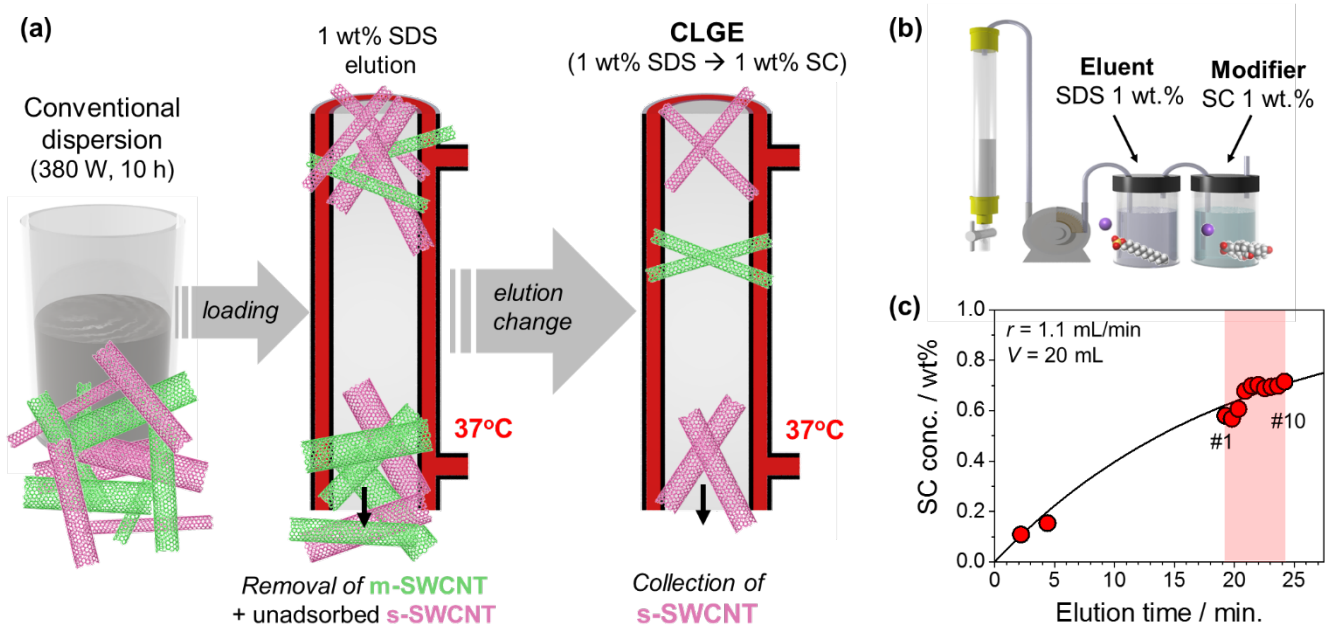
(a)
Conventional dispersion (380 W, 10 h)
loading
1 wt% SDS elution
37°C
Removal of m-SWCNT + unadsorbed s-SWCNT
elution change
CLGE
(1 wt% SDS → 1 wt% SC)
37°C
Collection of s-SWCNT
(b)
Eluent
SDS 1 wt.%
Modifier
SC 1 wt.%
(c)
r = 1.1 mL/min
V = 20 mL
#1
#10
SC conc. / wt%
Elution time / min.
0.0
0.2
0.4
0.6
0.8
1.0
0
5
10
15
20
25

Fig. 3.

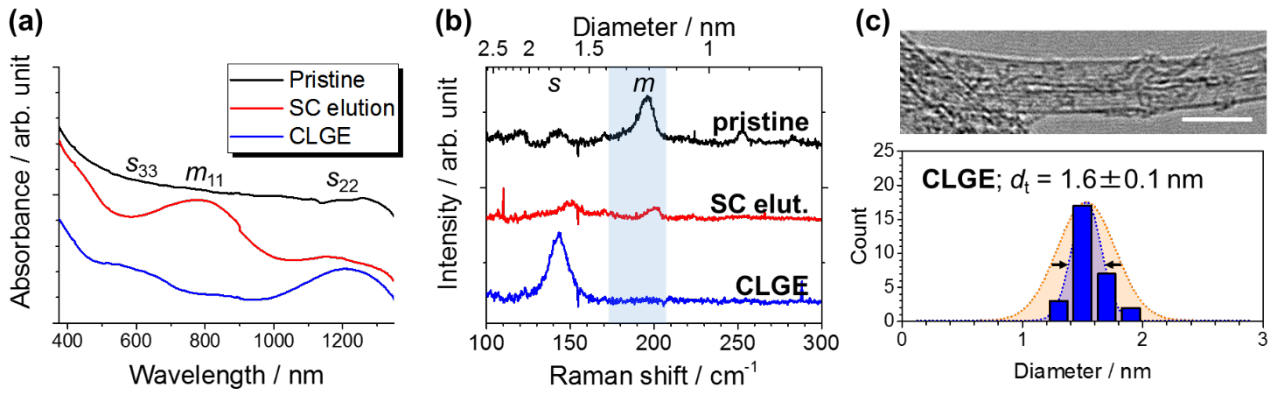
(a)
Absorbance / arb. unit
Pristine
SC elution
CLGE
s_{33}
m_{11}
s_{22}
400
600
800
1000
1200
Wavelength / nm
(b)
Diameter / nm
2.5
2
1.5
1
Intensity / arb. unit
s
m
pristine
SC elut.
CLGE
100
150
200
250
300
Raman shift / cm^{-1}
(c)
CLGE; d_t = 1.6±0.1 nm
Count
0
5
10
15
20
25
0
1
2
3
Diameter / nm

Fig. 4.

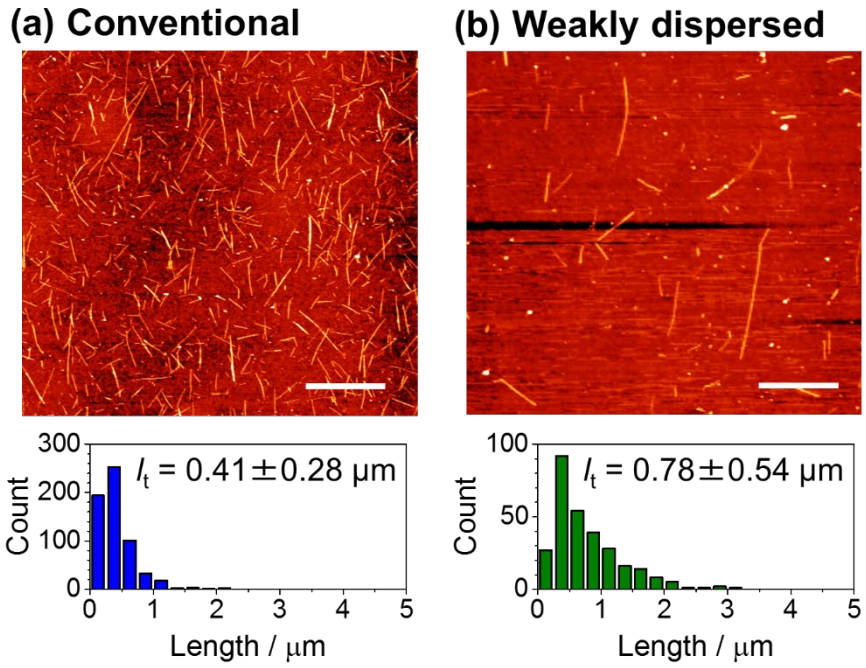
(a) Conventional
(b) Weakly dispersed
300
200
100
0
Count
l_t = 0.41±0.28 μm
0 1 2 3 4 5
Length / μm
100
50
0
Count
l_t = 0.78±0.54 μm
0 1 2 3 4 5
Length / μm

Fig. 5.

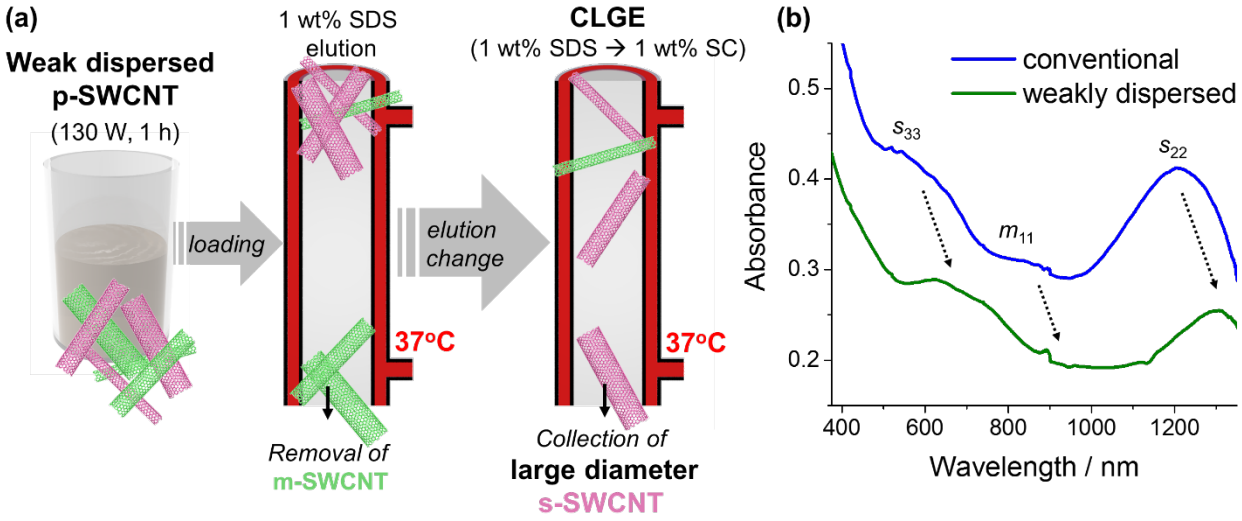
(a)
Weak dispersed
p-SWCNT
(130 W, 1 h)
loading
1 wt% SDS
elution
37°C
Removal of
m-SWCNT
elution
change
CLGE
(1 wt% SDS → 1 wt% SC)
37°C
Collection of
large diameter
s-SWCNT
(b)
conventional
weakly dispersed
s_{33}
m_{11}
s_{22}
Absorbance
0.5
0.4
0.3
0.2
400
600
800
1000
1200
Wavelength / nm

Fig. 6.

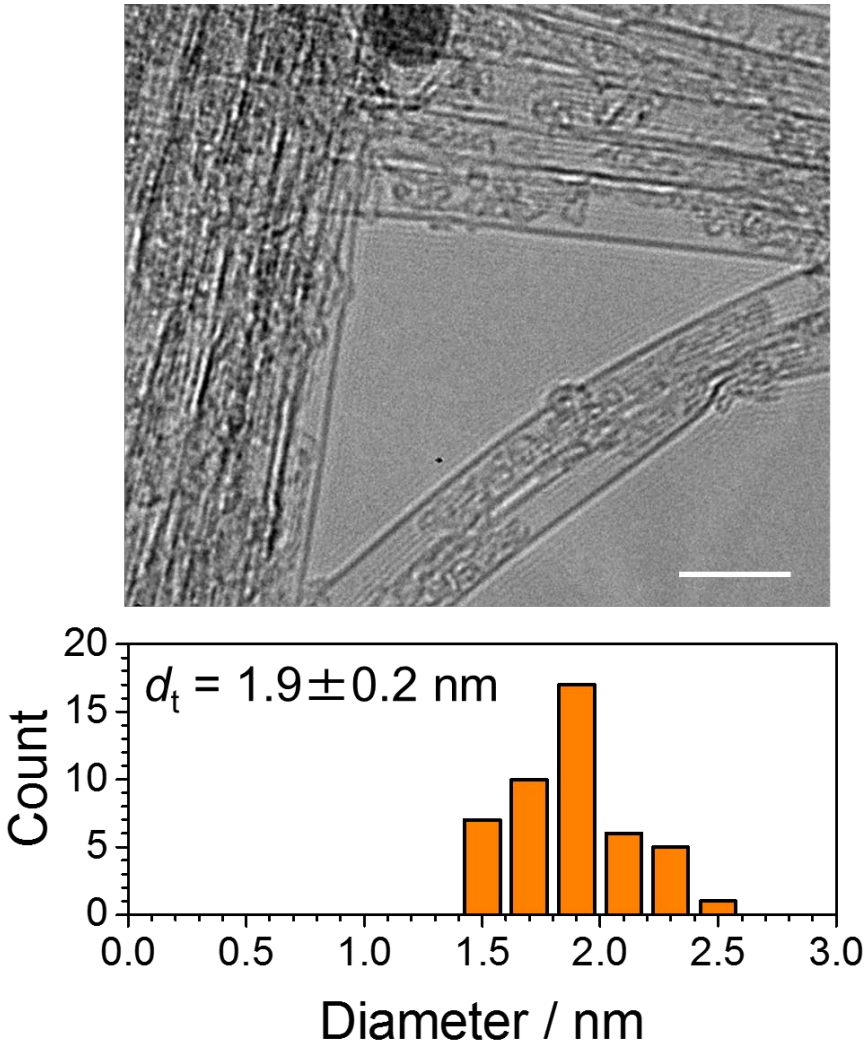

Fig. 7

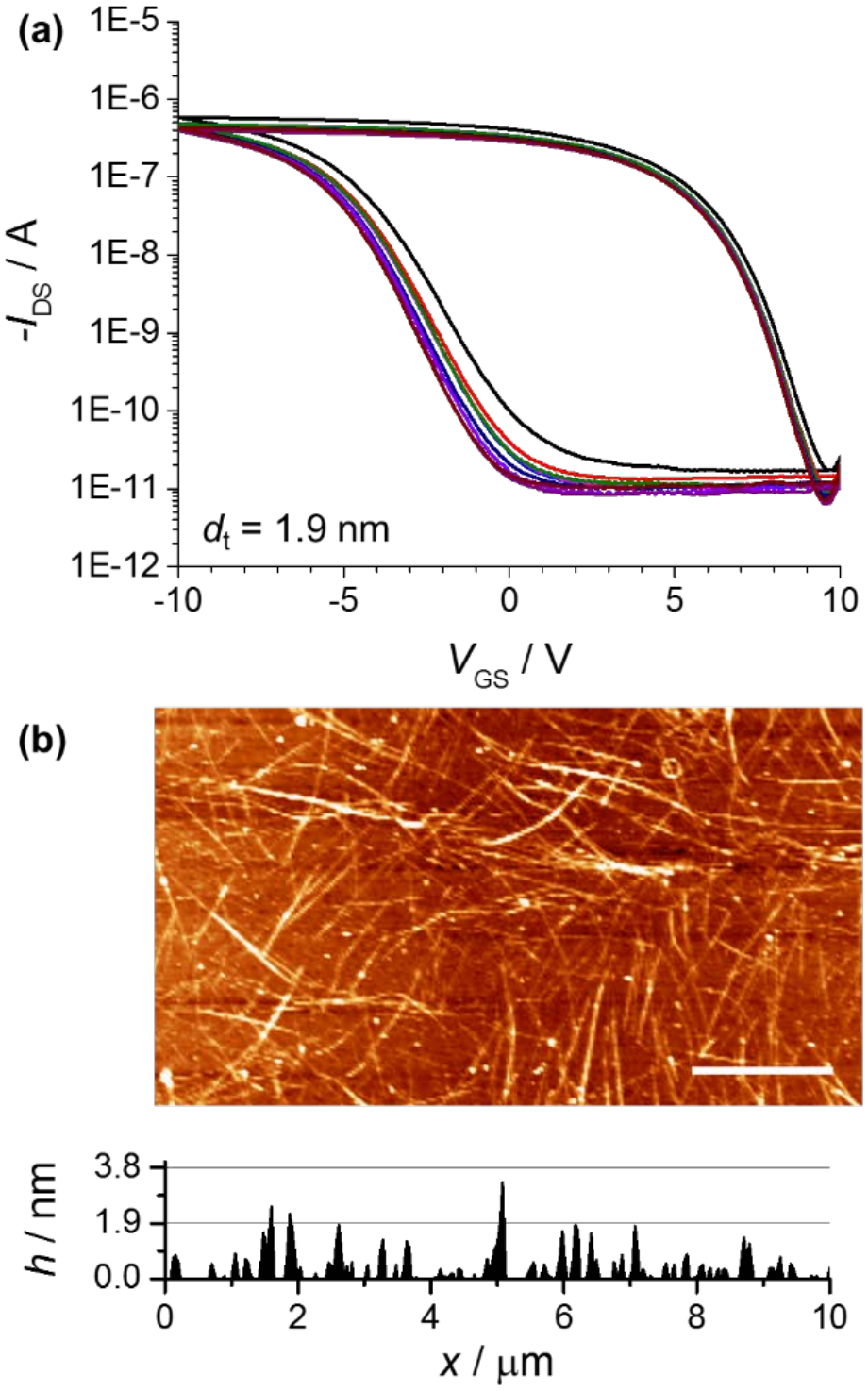
(a)
1E-5
1E-6
1E-7
1E-8
1E-9
1E-10
1E-11
1E-12
-I_DS / A
d_t = 1.9 nm
-10
-5
0
5
10
V_GS / V
(b)
3.8
1.9
0.0
h / nm
0
2
4
6
8
10
x / μm

Fig. 8.

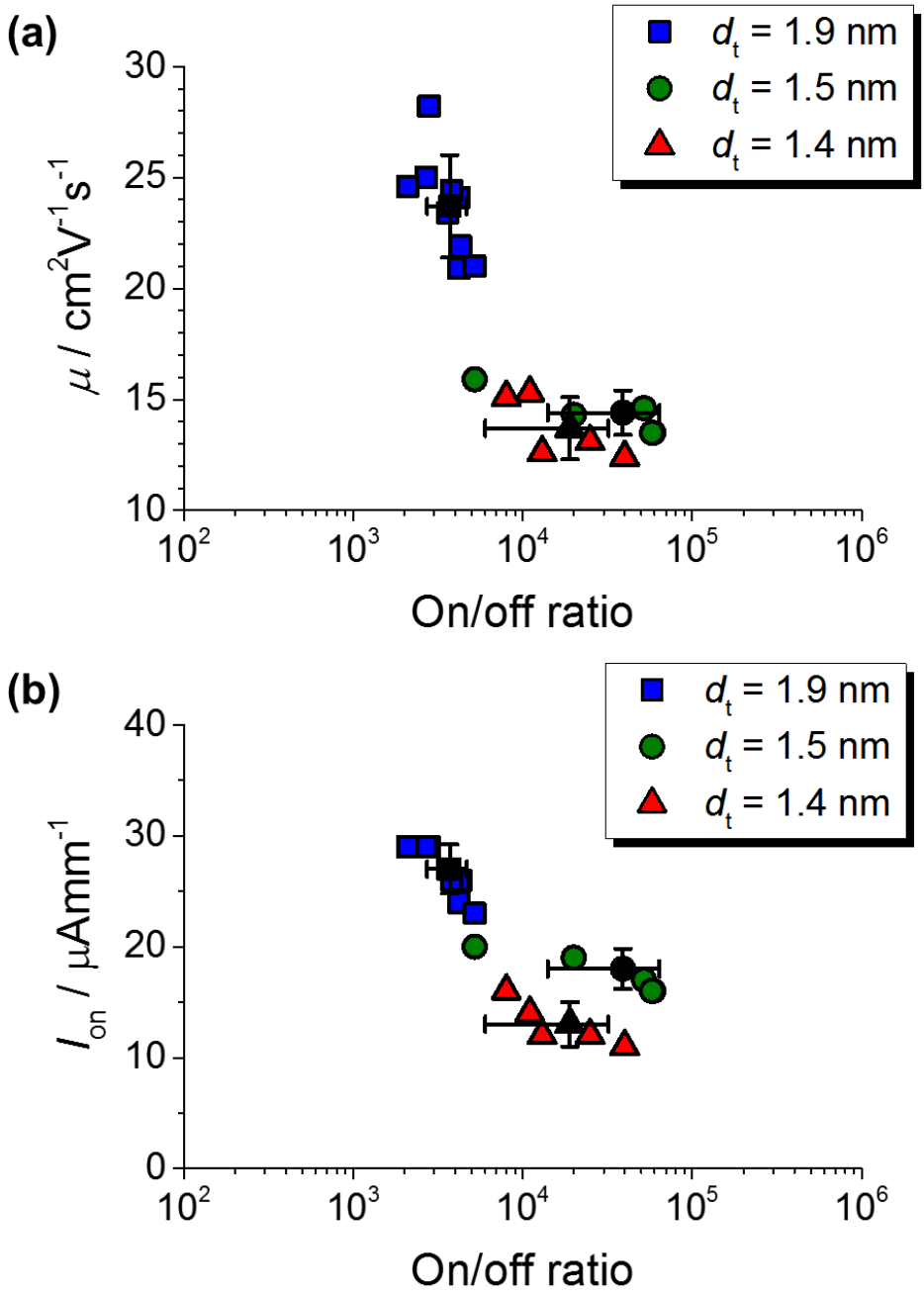
(a)
d_t = 1.9 nm
d_t = 1.5 nm
d_t = 1.4 nm
μ / cm^{2}V^{-1}s^{-1}
30
25
20
15
10
10^2
10^3
10^4
10^5
10^6
On/off ratio
(b)
d_t = 1.9 nm
d_t = 1.5 nm
d_t = 1.4 nm
I_{on} / μAmm^{-1}
40
30
20
10
0
10^2
10^3
10^4
10^5
10^6
On/off ratio

Fig. 9.